TU Delft

Delft University of Technology

Towards a particle based approach for multiscale modeling of heterogeneous catalytic reactors

Sengar, A.; Kuipers, J. A.M.; van Santen, R. A.; Padding, J. T.

DOI
10.1016/j.ces.2018.10.038

Publication date
2019

Document Version
Final published version

Published in
Chemical Engineering Science

Citation (APA)
Sengar, A., Kuipers, J. A. M., van Santen, R. A., & Padding, J. T. (2019). Towards a particle based approach for multiscale modeling of heterogeneous catalytic reactors. *Chemical Engineering Science*, *198*, 184-197. https://doi.org/10.1016/j.ces.2018.10.038

Important note
To cite this publication, please use the final published version (if applicable).
Please check the document version above.

Copyright
Other than for strictly personal use, it is not permitted to download, forward or distribute the text or part of it, without the consent of the author(s) and/or copyright holder(s), unless the work is under an open content license such as Creative Commons.

Takedown policy
Please contact us and provide details if you believe this document breaches copyrights.
We will remove access to the work immediately and investigate your claim.

This work is downloaded from Delft University of Technology.
For technical reasons the number of authors shown on this cover page is limited to a maximum of 10.

Chemical Engineering Science 198 (2019) 184–197

Contents lists available at ScienceDirect

Chemical Engineering Science

journal homepage: www.elsevier.com/locate/ces

Towards a particle based approach for multiscale modeling of heterogeneous catalytic reactors

A. Sengar [a,*], J.A.M. Kuipers [a], R.A. van Santen [b], J.T. Padding [c]

[a] Department of Chemical Engineering and Chemistry, Eindhoven University of Technology, P.O. BOX 513, 5600 MB Eindhoven, the Netherlands
[b] Institute for Complex Molecular Systems, Eindhoven University of Technology, P.O. Box 513, 5600 MB, Eindhoven, the Netherlands
[c] Process and Energy Department, Delft University of Technology, Leeghwaterstraat 39, 2628 CB, Delft, the Netherlands

HIGHLIGHTS

- Simulation of convection-reaction-diffusion for heterogenous catalytic reactors.
- Numerical computation of bulk mutual diffusivity using SRD.
- Incorporation of complex reaction systems while maintaining the interfacial physics.
- Dimensionless analysis to convey physical information between reactive systems.
- Different modeling examples show from linear systems to nonlinear reaction systems.

GRAPHICAL ABSTRACT

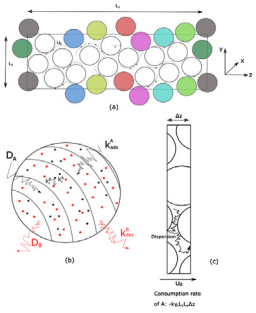

ARTICLE INFO

Article history:
Received 1 July 2018
Received in revised form 12 October 2018
Accepted 23 October 2018
Available online 27 October 2018

Keywords:
Heterogenous catalysis
Multiscale modelling
Stochastic rotation dynamics
Multicomponent diffusion
Nonlinear reactions
Unsteady state modelling

ABSTRACT

Particle based approaches are one of the recent modeling techniques to overcome the computational limitation in multiscale modeling of complex processes, for example a heterogeneous catalytic reactor. We propose an efficient model for a chemical reactor where hydrodynamics of the solvent is determined by Stochastic Rotation Dynamics and a reaction occurs over a catalytic surface where the reaction kinetics follows the mean-field assumption. We highlight the modeling techniques required to simulate such a system and then validate the model for its separate and combined components of convection, diffusion and reaction(s). A dimensionless analysis helps compare processes occurring at different scales. We determine the Reynolds number, *Re*, and the Damkohler numbers, *Da* and Da_L in terms of key quantities. The approach is then used to analyse a reaction (a) following the Langmuir-Hinshelwood kinetics, (b) generating product particles with different self-diffusivity values as compared to the reactant particles. The model developed can further incorporate reactions occurring inside complex geometries (pore diffusion) and also be used to study complex reaction systems for which the mean-field assumption is no longer valid.
© 2018 The Authors. Published by Elsevier Ltd. This is an open access article under the CC BY-NC-ND license (http://creativecommons.org/licenses/by-nc-nd/4.0/).

1. Introduction

The ability to model physical systems occurring at multiple time scales, with the current computational power at hand, has been extensively used to resolve or discover new phenomena mainly in the field of fluid and solid mechanics (Chen and Doolen, 1998; Steinhauser, 2007), polymers (Sheng et al., 2004), proteins (Kmiecik et al., 2016), and catalysis (Salciccioli et al., 2011).

Fluid dynamics and catalysis problems occur at comparably different time scales which makes it difficult to incorporate the complete information about one process while modeling the other and vice versa. In the field of Computational Fluid Dynamics, incorporating detailed reaction kinetics is helpful in improving the

* Corresponding author.
E-mail addresses: a.sengar@tue.nl (A. Sengar), j.a.m.kuipers@tue.nl (J.A.M. Kuipers), r.a.v.santen@tue.nl (R.A. van Santen), j.t.padding@tudelft.nl (J.T. Padding).

https://doi.org/10.1016/j.ces.2018.10.038
0009-2509/© 2018 The Authors. Published by Elsevier Ltd.
This is an open access article under the CC BY-NC-ND license (http://creativecommons.org/licenses/by-nc-nd/4.0/).

measurements of concentration distribution of reactants or products across the reactor system (Eigenberger, 2008; Kuroki et al., 2009; Wehinger et al., 2015). However, solution convergence at highly nonlinear conditions requires a very high grid resolution which slows down the whole scheme. Sengar et al. (2017) have previously shown that even a simple $A \rightarrow B$ reaction can show nonlinear dependence on reactant concentration under certain possible conditions.

Recent mesoscale modeling techniques, involving a particle based treatment of fluid, like Lattice Boltzmann method (LBM), Stochastic Rotation Dynamics (SRD), and Dissipative Particle Dynamics (DPD) offer an alternative approach in modeling these multiphysics problem. Treatment of particles in ensembles at different spatiotemporal scales reduces the total number of degrees of freedom inside the system, making it computationally more feasible. These modeling techniques, therefore, allow a faster implementation of detailed reaction kinetics coupled with fluid dynamics.

The field of particle based simulations has previously been used to study multiscale coupling involving flow and adsorption in porous media using a reactive Lattice Based scheme (Vanson et al., 2015), adsorption and diffusion in MetalOrganic Frameworks (Villemot et al., 2014), transport properties during convection-diffusion-reaction using DPD (Li et al., 2015). For the present work, we will employ SRD to simulate heterogeneous nonlinear reactions.

Stochastic Rotation Dynamics (SRD) (Malevanets and Kapral, 1999), uses a discrete-time dynamics of coarse-grained particles in a continuous space. The modeling scheme has previously been used to study single phase and multiphase flow problems (Tüzel et al., 2007; Padding and Louis, 2006), homogenous (Rohlf et al., 2008) and heterogenous (Tucci and Kapral, 2004; Huang et al., 2016) catalytic reaction systems with (Sengar et al., 2017) incorporating a Langmuir Hinshelwood reaction kinetics over the surface of a catalytic strip.

Study of a heterogeneous chemical reaction in a fixed bed reactor involves the resolution of three primary processes, convection, reaction, and diffusion at unsteady state. To simulate the reaction step, the complete reaction cycle is broken down into individual reaction steps like adsorption, desorption and surface reaction (Sengar et al., 2017). This makes it convenient to observe the effects of any intermediary reaction process on the bulk fluid mixture by making the other processes fast enough.

As the number of participating components in the system increases, the classical definition of self diffusion coefficient, according to Fickian Diffusion, is not enough (Krishna and Wesselingh, 1997; Taylor and Krishna, 1993). Further, for reactions involving gases, a difference in number of moles of products and reactants will result in an internal pressure gradient which can still be accounted for in the mutual diffusivity at unsteady state or a pseudo steady state. We incorporate all these effects in the Maxwell-Stefan diffusivity.

In Section 2.1, we briefly discuss the particle-particle interactions in SRD followed by a description of the numerical techniques, Section 2.2, to calculate the Maxwell-Stefan diffusivity for a binary mixture of SRD particles with different mass leading to different self-diffusivity. A set of dimensionless parameters are defined in Section 3.1 to optimize the processes occurring at different time and length scales, treated in subsequent Sections 3.2, 3.3, 3.4, 3.5. We first perform a cold flow analysis on flow around a sphere, Section 3.2, and pressure drop across a packed bed, Section 3.3, to validate the viscous and convective coupling in an SRD fluid in the presence of spherical obstacles. This is followed by the introduction of a chemical reaction on the surface of the spheres and introduction of three dimensionless numbers, which are the Damkohler numbers Da and Da_L, and the Peclet number Pe_L. The model is validated for reaction-diffusion coupling over a catalytic sphere placed in a pool of reactant in Section 3.4. In Section 3.5, we finally combine the three processes convection, diffusion and reaction, and analyse the net conversion as a function of the above

Table E.5
List of symbols in order of appearance in the manuscript.

a_0	SRD unit cell [m]	N_s	Number of spheres in simulation setup
k_B	Boltzmann constant [kg m^2 s^{-2} K^{-1}]	θ	Vacancy fraction over the sphere surface
m_i	Mass of single SRD particle of species i [kg]	θ_i	Fraction of species i over sphere surface
Δt_c	Hydrodynamic time step [s]	p^i_{ads}	Probability of adsorption of species i on sphere surface
α	SRD rotational angle	p^i_{des}	Probability of desorption of species i from sphere surface
γ_i	Number of species i particles per unit SRD cell [m^{-3}]	p^i_r	Probability of reaction of species i on sphere surface
D_i	Self-diffusivity of species i [m^2 s^{-1}]	N_{cat}	Number of catalytic sites on a single sphere
$\mathbf{d}_i$	Friction force per particle of species i [m^{-1}]	k^i_X	Rate constant for surface process X occurring for particle i per area of catalyst surface. Adsorption: [m s^{-1}], Desorption, Reaction: [m^{-2} s^{-1}]
μ_i	Chemical potential of particle of species i [kg m^2 s^{-2}]	K^i_{eq}	Adsorption-desorption Equilibrium constant for species i [m^3]
χ_i	Number fraction of species i	Da	Damkohler number
T	Temperature [K]	D_L	Longitudinal dispersion coefficient [m^2 s^{-1}]
$\mathbf{u}_i$	Average velocity of particles of species i [m s^{-1}]	τ'	Tortuosity of packed bed column
$\mathbf{F}_i$	External force on single particle of species i [kg m s^{-2}]	u	Average velocity of solvent in packed bed column [m s^{-1}]
$\mathbf{a}_i$	Acceleration because of external force on particle of species i [m s^{-2}]	t_{start}	Initial run time of simulation setup to achieve mechanical equilibrium [s]
v_i	Velocity of individual particle of species i [m s^{-1}]	k	Volumetric reaction rate constant [m^3 s^{-1}]
N_i	Number of SRD particle of species i	A_{cat}	Area of single catalytic sphere [m^2]
D_{ij}	Mutual diffusivity between species i and j [m^2 s^{-1}]	Da_L	Damkolher number along the longitudinal direction of simulation setup
D^o_{ij}	Pure mutual diffusivity between species i and j [m^2 s^{-1}]	Pe_L	Peclet number along the longitudinal direction of simulation setup
ρ_i	Mass density of species i [kg m^{-3}]	L'_z	Buffer length in the simulation setup where reaction occurs [m]
R	Radius of sphere used in simulation setup [m]	Sc	Schmidt number
η_i	Viscosity of species i [kg m^{-1} s^{-1}]	$\gamma_{i,l}$	Local number density of species i over catalytic sphere [m^{-3}]
Re	Reynolds number	β	Number of strips on a single reaction sphere
ϵ	Gas porosity	A'	Area of a single strip [m^2]
u_s	Superficial velocity [m s^{-1}]	J_i	Diffusive flux of species i [m^{-2} s^{-1}]
P	Pressure [kg m^{-1} s^{-2}]	γ_t	Total number density of all particles per unit cell [m^{-3}]
L_i	Reactor length along $i = x, y, z$ direction [m]	$[B]$	Diffusion matrix [m^{-2} s]
f	Dimensionless pressure drop per unit length	ω_i	Mass fraction of species i

mentioned dimensionless numbers. In the next Section 4, we highlight two reaction scenarios where we cannot assume a constant value of above mentioned dimensionless number across the reactor length. We end with a Conclusion section on the scalability of the work while incorporating complex reaction mechanisms. All symbols used within the text are mentioned, with theri dimensions, in Table E.5.

2. Model development

The previous study (Sengar et al., 2017) highlights the use of SRD with reaction kinetics to model simple heterogeneous chemical reactions in a micro reactor. Reactants and products were considered with equal mass and equal diffusivity. The further model development in this work is divided into two parts. The first part talks about the inclusion of characteristically distinct reaction species and obtaining the mutual diffusivity for such a system while the second part explores the geometry of fluid-solid interface as compared to the planar geometry in Sengar et al. (2017).

2.1. Stochastic rotation dynamics

Each participating species of the initial reaction mixture is represented by a system of point-like particles. The system starts with homogeneously distributed N particles with number fraction and mass of particle of each species being χ_i and m_i respectively. The 3D space is discretized into a cubic lattice of size a_0 and time is discretized into time intervals of Δt_c which governs the displacement of particles before successive collisions.

Streaming of particles occurs according to the Euler scheme, $\mathbf{r}_i^{t+1} = \mathbf{r}_i^t + \mathbf{v}_i^t \Delta t_c$, where $\mathbf{r}_\mathbf{i}^t$ and $\mathbf{v}_\mathbf{i}^t$ are the position and velocity vectors of particle i at time t. The second step is the velocity update which occurs according to the collision rule $\mathbf{v}_i^{t+1} = \bar{\mathbf{v}} + \boldsymbol{\Omega}(\mathbf{v}_i^t - \bar{\mathbf{v}})$. $\bar{\mathbf{v}}$ is the center-of-mass velocity of all particles sharing the same cell and Ω is a stochastic rotation matrix that rotates the velocities by a fixed angle α while conserving energy and momentum.

To ensure Galilean invariance (Ihle and Kroll, 2003), a random grid-shift procedure (Ihle and Kroll, 2001) is employed. The origin of the lattice is displaced by a stochastic 3D vector (which is same for all lattices per time step) whose magnitude of each Cartesian component is defined by a random number between 0 and a_0. To account for the under filling of cells near boundaries caused by the grid-shift procedure, introduction of ghost particles for single solvent species (Lamura et al., 2001) was suggested which was expanded to preserve momentum when multiple components might be present in such cells (Sengar et al., 2017). To maintain the system at fixed temperature even in the presence of external forces, a Galilean invariant thermostat (Padding and Louis, 2006), that rescales particle velocities in the center-of-mass velocity frame of their cell, is used.

Transport coefficients like viscosity and diffusion coefficient for single species solvents have extensively been studied in Ihle and Kroll (2003), Tüzel et al. (2003, 2006), Kikuchi et al. (2003), Gompper et al. (2009), Noguchi and Gompper (2008), Pooley and Yeomans (2005). For a single SRD particle species, the diffusion coefficient is written in a parametric form as

$$\frac{D}{D_0} = \frac{k_B T \Delta t_c}{2m}\left(\frac{3\gamma}{(\gamma - 1 + e^{-\gamma})(1 - \cos\,\alpha)} - 1\right) \tag{1}$$

m, k_BT and D_0 are the units used to parameterize the physical parameters in SRD, Table 1. When $\alpha = 0^\circ$, the particles do not change their trajectories upon collision as a result of which $D \to \infty$. When $\alpha = 180^\circ$, particles face an inversion of velocity representing a condition with minimum possible diffusivity, D. As the number of particles in the grid cell (γ) increases, a single particle will face more collisions within a single time step, reducing the diffusivity. However, as γ increases, there is a saturation and for $\gamma \to \infty$, the diffusivity expression becomes independent of γ.

Table 1
Simulation parameters used and their units.

Unit	Expression
Length	a_0
Energy	k_BT
Mass of solvent	m_0
Time	$t_0 = a_0\sqrt{\frac{k_BT}{m_0}}$
[7pt] Diffusion coefficient	$D_0 = \frac{a_0^2}{t_0} = a_0\sqrt{\frac{k_BT}{m_0}}$
Fluid Simulation parameters	
γ: average number of particles per grid cell	
Δt_c: SRD streaming time step	
α: SRD rotation angle	

2.2. Diffusivity in multi-component mixtures

When a solution consists of more than one component, the mutual interaction between particles is described by a mutual diffusivity. For systems representing ideal gases with low interaction between particles of different components, a Fickian definition of mutual diffusivity is used. However, for real fluids when cross-interaction terms dominate, a Maxwell-Stefan approach is necessary. Maxwell-Stefan diffusivity for multicomponent mixtures has been studied previously using Molecular Dynamics, see e.g. van de Ven-Lucassen (1998). In this work, we will use a similar approach to analyse binary mixtures.

The force acting on a single particle of species i in an SRD mixture with n components, at a constant temperature T can be written as the gradient of chemical potential, μ_i (van de Ven-Lucassen, 1998; Taylor and Krishna, 1993)

$$\mathbf{d}_i = -\nabla_T \mu_i = \sum_{j=1}^{n} \chi_j \frac{kT}{D_{ij}}(\mathbf{u_j} - \mathbf{u_i}) \tag{2}$$

$\mathbf{u_i}$ and χ_i are the average velocity and mole fraction of species i respectively. The solution obeys the ideal gas law $PV = Nk_BT$, where N is the total number of particle of all species. In presence of an external field $\mathbf{F}_i$, the net force on a single particle is $\mathbf{F}_i - \nabla_T \mu_i$. The above interpretation of D_{ij} can be obtained from a non-equilibrium or an equilibrium approach.

2.2.1. NEMD approach

The Non-Equilibrium Molecular Dynamics approach (Berendsen, 1991) works by applying equal and opposite external forces on different components in a solution mixture such that the net external force is zero and therefore the net momentum across all particles remains conserved at each discrete time step. For a binary mixture, the approach can be simplified and force and momentum conservation equation can respectively be written as

$$Nm_1\chi_1\mathbf{a_1} + Nm_2\chi_2\mathbf{a_2} = 0 \tag{3a}$$
$$Nm_1\chi_1\mathbf{u_1} + Nm_2\chi_2\mathbf{u_2} = 0 \tag{3b}$$

$\mathbf{a_i}$ is the force acting on particles of species i. For small external forces, the velocity response is

$$\frac{d\mathbf{u_1}}{dt} = \mathbf{a_1} + \frac{k_BT\chi_2}{m_1 D_{12}}(\mathbf{u_2} - \mathbf{u_1}) \tag{4a}$$
$$\frac{d\mathbf{u_2}}{dt} = \mathbf{a_2} - \frac{k_BT\chi_1}{m_2 D_{12}}(\mathbf{u_2} - \mathbf{u_1}) \tag{4b}$$

The factor k_BT/D_{12} represents the mutual mobility between species 1 and 2 caused by internal friction. The coupled differential

equations can be solved exactly to get the terminal velocity of particles under this external force. For $t \to \infty$, the terminal velocity of species 1 is

$$\mathbf{u_1}(\infty) = \frac{\mathbf{a_1} m_1 m_2 D_{12}}{k_B T(m_1\chi_1 + m_2\chi_2)} \tag{5}$$

For sufficiently small external forces, we therefore expect a linear dependence of terminal velocity of a species on the force applied, which can be used to calculate the value of the mutual diffusion coefficient D_{12}.

2.2.2. Green-Kubo relations

Another approach is by employing linear response theory in statistical mechanics. It has been shown (van de Ven-Lucassen, 1998) that the velocity response of a solvent in presence of another species can be used to estimate the Green-Kubo relation for the Maxwell-Stefan diffusion coefficient as

$$D_{12} = \frac{\chi_2}{3N_1}\int_0^\infty \left\langle \left[N_2\sum_{i=1}^{N_1} v_1^i(0) - N_1\sum_{j=1}^{N_2} v_2^j(0)\right] \cdot \left[N_2\sum_{k=1}^{N_1} v_1^k(t) - N_1\sum_{l=1}^{N_2} v_2^l(t)\right]\right\rangle dt \tag{6}$$

If cross-species velocity terms are neglected, we get the pure mutual diffusion coefficient D_{12}^o.

$$D_{12}^o = \frac{\chi_2}{3}\int_0^\infty \langle \mathbf{v_1}(0).\mathbf{v_1}(t)\rangle dt + \frac{\chi_1}{3}\int_0^\infty \langle \mathbf{v_2}(0).\mathbf{v_2}(t)\rangle dt \tag{7}$$

$\mathbf{v_i}$ refers to velocities averaged over the entire species.

Simulations were carried out to calculate the diffusion coefficient from the above two approaches which serves as a validation for the SRD description of particles.

2.2.3. Measurement of mutual diffusion coefficient expressions

For the NEMD approach, the system was initialized with an equimolar binary mixture of particles with mass m_1 and m_2. The self-diffusivity coefficients of these particles are in ratio $D_1/D_2 = m_2/m_1$. In Fig. 1, the terminal velocity of particles of type 1 is calculated versus an applied force $\mathbf{a_1}$. $m_1 = 1$ and m_2 takes values $0.2, 0.5, 1.0, 2.0$. When $m_2 = 1.0$, the D_{12} value obtained from the slope is equal to the self-diffusivity coefficient of both particles 1 and 2.

To calculate the mutual diffusion coefficient using the Green-Kubo relation Eq. (6), 2 species of mass $m_1 = 0.5$ and $m_2 = 1.0$ are chosen. The number fraction of species 1 is varied from 0 to

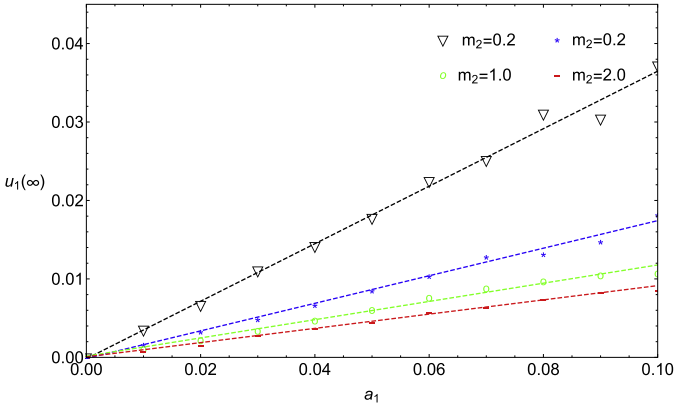

Fig. 1. Terminal velocity of particles of type 1 versus force applied in presence of particles of type 2 with mass m_2, Eq. (5). From the slope of the above, we can obtain the mutual diffusion coefficient D_{12}. $\chi_1 = \chi_2 = 0.5, \Delta t_c = 0.1, k_B T = 1.0, a_0 = 1.0$.

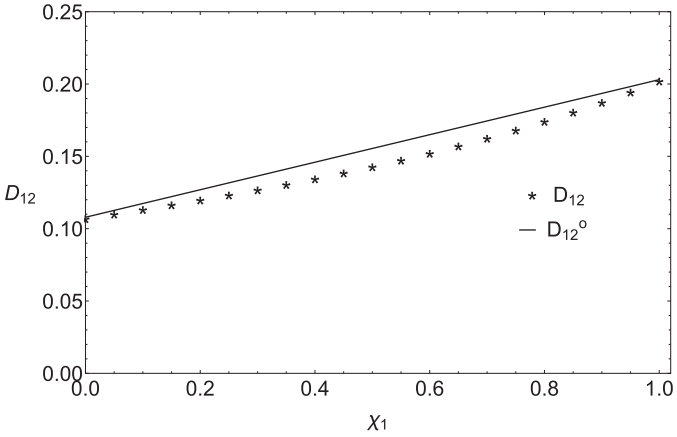

Fig. 2. Variation of mutual diffusivity as a function of χ_1. Straight line is the pure mutual diffusivity, D_{12}^o (Eq. (7)), and starred line is D_{12} (Eq. (6)).

1 and the velocity correlation functions for both particles are calculated to estimate the mutual diffusivity D_{12}. This is shown in Fig. 2.

The linear curve D_{12}^o is the pure mutual diffusion coefficient when no cross-correlation terms are included. The higher the difference between D_{12} and D_{12}^o, the more the different species interact and act like non-ideal mixtures. The difference is maximum when $\chi_1 = 0.5$.

3. Convection, diffusion and reaction across spheres

For the next part of the work, we define a sphere, the surface of which may be reactive or not. We will then study the flow properties of a fluid around this sphere as a function of its Reynolds number *Re*. This is followed by a methodology to incorporate reactions over the surface and the conditions under which a linear approximation for reaction can be done. The linear treatment of reaction is then used to verify (a) the change in flux of the reactant species over the sphere with time, and (b) conversion in a packed-bed reactor with dispersion.

3.1. Dimensionless analysis

In a reactor, the three main processes namely convection, reaction and diffusion never occur at the same time scale. It is convenient in such multiscale systems to measure the variables of a process *X* occurring at a time scale with respect to the variables of another process *Y* at a different time scale. We, thus, define characteristic dimensions, at a characteristic time scale, to analyze any variable of any process at any time scale.

The three dimensions chosen are the radius of a single sphere *R*, self-diffusion coefficient of initial solvent species D_A, and the

Table 2
Physical quantities with their dimensions

Physical Quantities	Dimensions
Length	R
Diffusion	D_A
Viscosity	η_A
Time	$\frac{R^2}{D_A}$
Mass	$\frac{\eta_A R^3}{D_A}$
Energy	$\eta_A R D_A$
Velocity	$\frac{D_A}{R}$
Number Density	R^{-3}
Pressure	$\frac{\eta_A D_A}{R^2}$
Mass Density	$\frac{\eta_A}{D_A}$

viscosity of the solvent η_A. Since we treat a single SRD particle as part of an ideal fluid, the ideal-gas law is obeyed $PV = Nk_BT$ with N being the number of SRD particles. Physical quantities and their dimensions are shown in Table 2. For any physical quantity $\mathbf{X}$, we will represent the corresponding dimensionless quantity as $\mathbf{X^o}$.

3.2. Flow across a sphere

Lamura et al. (2001), Allahyarov and Gompper (2002) have previously shown the use of SRD to model flow past a circular and square 2D cylinder and 3D spheres. Here we will first verify our implementation, by comparing the predicted flow field around a 3D sphere with their results.

The system consists of a sphere of radius R present in a box of dimensions L_x, L_y, L_z with the sphere center at $L_x/2, L_y/2, L_z/4$. The boundaries of the simulation box are periodic and the surface of the sphere has no-slip boundary conditions. To ensure that the periodic boundaries do not affect the hydrodynamics of the system, we choose $L_z > L_x, L_y \geqslant 10R$ (z being the direction of flow). An SRD fluid A is present inside the box at $t = 0$. For all $t > 0$, a constant pressure difference between $z = 0$ and $z = L_z$ is applied leading to a flow along the z direction. When mechanical equilibrium is established, the velocity profile of the fluid along the z-direction can be studied. For small values of $Re = \rho_A v_{max}(2R)/\eta_A$ (in dimensionless units $Re = 2\rho_A^o v_{max}^o$), the velocity vectors are streamlined over the surface of sphere. As Re increases, a recirculation region is formed behind the sphere (Churchill, 1988) followed by vortex shedding (Taneda, 1956) for $Re > 200$.

To avoid slip of the velocity field at the sphere surface caused by low number density of particles in cells near the surface, a bulk fill rule for such cells has been implemented. For details, we refer to Appendix A.

The size of the wake region is defined as the length of the region with a negative time-averaged velocity behind the sphere. In Fig. 3, we compare the results obtained from our SRD model with those of Allahyarov and Gompper (2002) and the experimental data (Taneda, 1956). Between $20 < Re < 100$, the graph shows a monotonous increase in the wake length which is in good agreement with established results.

3.3. Pressure drop in a packed column

The wake formation behind a sphere depicts a phenomenon where coupled convection and viscosity effects cause disturbance in the flow of fluid behind a sphere. The fluid faces resistance in its path leading to pressure difference at difference faces of the sphere along the direction of fluid flow. In a packed-bed arrangement of spheres, this pressure difference adds up and for laminar flows at relative low Re, the pressure drop per unit length of the reactor can be correlated by the Kozeny-Carman relation

$$\frac{\Delta P}{L_z} = 150\,\frac{\eta_A u_s}{(2R)^2}\,\frac{(1-\epsilon)^2}{\epsilon^3} \tag{8}$$

where u_s is the superficial velocity of fluid in the reactor and ϵ is the gas porosity. The above equation can be non-dimensionalized according to Table 2 as follows:

$$f = \frac{\Delta P}{L_z}\,\frac{R^3}{\eta_A D_A} = 75\,\frac{u_s R}{2D_A}\,\frac{(1-\epsilon)^2}{\epsilon^3} = \frac{75Re}{4\rho_A^o}\,\frac{(1-\epsilon)^2}{\epsilon^3} \tag{9}$$

where ρ_A^o is the dimensionless mass density and Re can also be written as

$$Re = 2\rho_A^o u_s^o \tag{10}$$

To model this pressure drop, we consider an open-boundary 3D box (L_x, L_y, L_z) with N_s spheres randomly placed inside. A periodic boundary system ensures no wall-effects are included. Spheres lying close to the boundaries are wrapped around to contribute to the packed column, see Fig. 5. The SRD fluid is placed around the spheres at $t = 0$. The SRD particles are then given an acceleration g along the +z-axis. The mean free path of SRD particles should remain comparable or smaller than the smallest distance between spheres inside the packed column. This will ensure that the continuum approximation (Knudsen number $\ll 1$) will still be valid in these simulations.

At mechanical equilibrium, the hydraulic pressure drop per unit length will be equal to the net force density on all SRD particles inside the packed column is $\Delta P/L = \rho_A g$.

We can thus study the response of an independent acceleration g on the dependent variable u_s, according to $f = \rho_A^o g^o$, where f is given by Eq. (9).

Fig. 4 plots the dimensionless pressure drop f as a function of Re and compares the results from the simulations for different bed porosities ϵ. Dashed lines represent the dimensionless Kozeny-Carman relation and the inverted triangles are the points obtained from SRD results. The match is quite good which shows that the fluid hydrodynamics at low porosities can be efficiently modeled by our current approach.

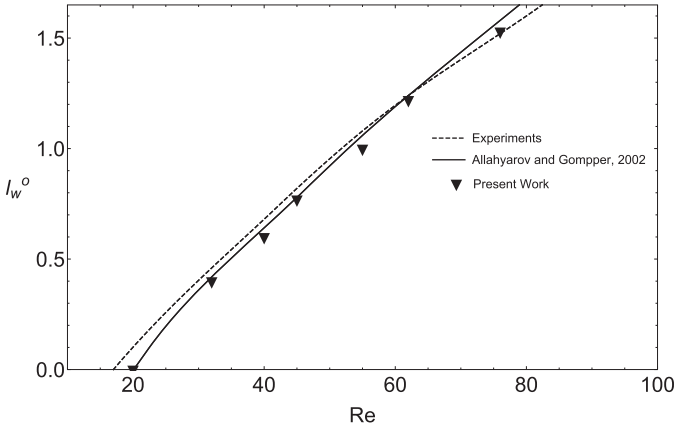

Fig. 3. The length of wake behind the sphere as a function of Re.

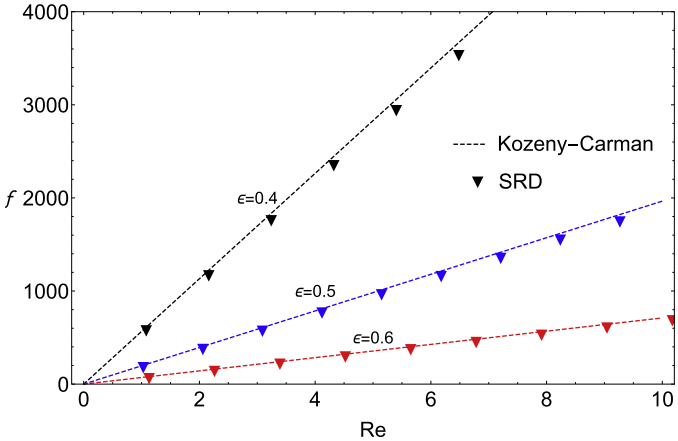

Fig. 4. Dimensionless pressure drop as a function of particle Reynolds number, Re, for $\epsilon = 0.4, 0.5, 0.6$. For each curve, g^o is varied to obtain a u_s^o which determines Re. Simulation parameters in terms of SRD units, Table 1: $\gamma_A = 20a_0, \Delta t_c = 0.1t_0, m_A = 1.0\sqrt{k_BT/m_0}, N_s = 150, L_z = 300a_0, L_x = L_y = 50a_0$.

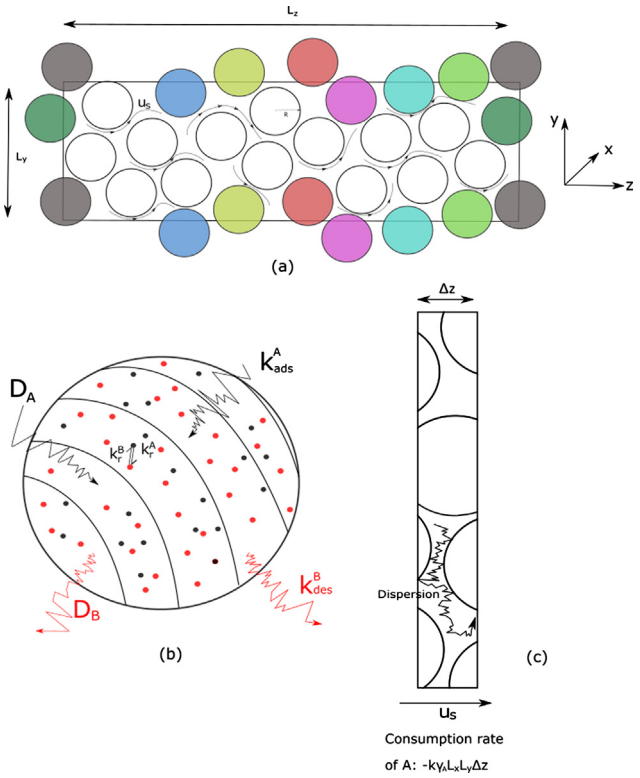

Fig. 5. 2D schematic of the 3D model reactor. (a) Reactor has periodic boundaries in 3 directions. Pressure different is applied across $z = 0$ and $z = L_z$ to induce a flow in $+z$ direction. Periodic images of the spheres overlapping with the periodic boundaries are indicated in color. (b) Schematic of reaction mechanism over the catalytic sphere. Each sphere has N_{cat} catalytic strips along the direction of flow. k_r^i are the reaction rates of adsorbed species i. (c) Inside a volume element of length Δz, the consumption rate of reactants is a sum of individual reactions occurring inside the volume.

3.4. Irreversible reaction on a sphere

The SRD model developed was validated (Sengar et al., 2017) for a reaction-diffusion case with reaction over a thin catalytic strip. We incorporated Langmuir-Hinshelwood kinetics for a $A \rightleftharpoons B$ reaction and estimated the product concentration profile based on Damkohler numbers when any single participating process in the reaction cycle(adsorption, desorption or site reaction) was rate determining. It was established that a linear assumption of reaction is only valid when adsorption of reactant species over the catalytic surface will be the rate determining step.

The following validation cases demonstrate application of an SRD based fluid in a system with convection, diffusion and reaction occurring at different time scales.

We first consider an example of a sphere placed in an infinite bath of reacting solvent A such that a linear reaction occurs at the surface of a sphere, Lu et al. (2018). The competing processes are the reaction of A at the surface which leads to a local concentration gradient causing an incoming diffusion flux of A. Diffusion and reaction compete in this unsteady state process.

To simulate this process, a sphere of radius R is placed in the center of the simulation box. In this example, the surface of the sphere is one single reactive strip since absence of convection ensures the system is isotropic, Appendix A.

The surface of the sphere, with area A_s, consists of N_{cat} reactive sites that are either vacant (with surface fraction θ) or contain adsorbed species i with surface fraction θ_i. Fluid particles of species i hitting the catalytic strip, within a time step Δt_c can adsorb with a probability p^i_{ads} which relates to the adsorption rate constant k^i_{ads},

Table 3
Independent, dependent and derived parameters in the model.

Input parameter	Expression
Sticking probability	p^i_{ads}
Desorption probability	p^i_{des}
Reaction probability	p^i_r
Number of catalyst sites	N_{cat}
Output parameter	**Expression**
Total number of adsorbed particles of species i	$N_{cat}\theta_i$
Total number of vacant sites on catalyst	$N_{cat}\theta$
Derived Rate constants	**Expression**
Adsorption rate	$k^i_{ads} = \sqrt{\frac{k_b T}{2\pi m_i}} p^i_{ads}$
Desorption rate	$k^i_{des} = \frac{-\ln(1-p^i_{des})}{A_{cat}\Delta t_c}$
Reaction rate	$k^i_r = \frac{-\ln(1-p^i_r)}{A_{cat}\Delta t_c}$
Equilibrium constant	$K^i_{eq} = \frac{k^i_{ads}}{k^i_{des}}$

see Table 3. A successful adsorption reduces the fractional vacancy θ of the catalyst by $1/N_{cat}$ while increasing θ_i by $1/N_{cat}$. Adsorbed particles stay at their positions, representing a surface-diffusion limited process. During the time step Δt_c, particles of species i may desorb from the surface or further react with probabilities p^i_{des} or p^i_r that relate to the rate constants of desorption and reaction, see Table 3. The global thermostat, Section 2.1, ensures the reaction is treated isothermally.

For all $t > 0$, A is adsorbed on the surface of the sphere with a probability p^A_{ads}. As described above, adsorbed A, with a fractional occupancy θ_A over the catalytic strip, can further desorb (with probability p^A_{des}) or react (with probability p^A_r) to form adsorbed species B, with surface fraction θ_B. Adsorbed B can further desorb (with probability p^B_{des}) or react back to form adsorbed A (with probability p^B_r). Desorption resulting in bulk particles of B can re-adsorb with a probability p^B_{ads}. For a linear irreversible reaction assumption, $p^A_{des} = p^B_{ads} = p^B_r = 0$ and $p^A_r = p^B_{des} = 1.0$, (Sengar et al., 2017). Such a probability parameter set also ensures that the catalytic surface itself will not have its own inherent time scale since it will be equilibrated almost instantly. Refer to Appendix B for a detailed description of coupling reactions with the bulk.

The reaction at the surface of the sphere gives rise to a concentration gradient leading to a diffusive flux of the reactant towards the catalyst, further fueling the reaction. The surface reactive boundary condition (Collins and Kimball, 1949) is

$$D_{AB}\left.\frac{\partial \gamma_A(r,t)}{\partial r}\right|_{r=R} = k^A_{ads}\gamma_A(t) \tag{11}$$

D_{AB} is the time varying mutual diffusivity of A and B near the catalytic surface since the process is at an unsteady state. If the catalytic strip achieves a steady state almost instantaneously, no concentration depletion region is formed near the sphere and the total number density of particles over the sphere always remains a constant. In this simple example, since particles A and B are only distinguishable by a tag, $D_{AB} = D_A$.

Lu et al. (2018) have presented an analytical solution for the number density $\gamma_A(r,t)$ of reactant species A in the region surrounding the sphere.

$$\frac{\gamma_A(r^o,t^o)}{\gamma_A(1,0)} = 1 - \frac{Da}{r^o(1+Da)}\left[\mathrm{erfc}\left(\frac{x}{2\sqrt{\tau}}\right) - e^{\tau+x}\mathrm{erfc}\left(\frac{2\tau+x}{2\sqrt{\tau}}\right)\right] \tag{12a}$$

$$\tau = (1+Da)^2 t^o, \quad x = (1+Da)(r^o-1) \tag{12b}$$

where $\gamma_A(1,0)$ is the constant number density of A in the region outside the sphere, $r > R$, at $t = 0$. The Damkohler number Da is equal to dimensional-less rate constant $k^{A,o}_{ads}$.

For $x = 0, r^o = 1$, close to the surface of the sphere, Eq. (12) becomes

$$\frac{\gamma_A(1,t^o)}{\gamma_A(1,0)} = 1 - \frac{Da}{(1+Da)}\left[1 - e^{\tau}\mathrm{erfc}(\sqrt{\tau})\right] \tag{13}$$

At steady state, $\lim \tau \to \infty$,

$$\frac{\gamma_A(1,t^o)}{\gamma_A(1,0)} = \frac{1}{1+Da} \tag{14}$$

For a reaction limited case, $Da \ll 1$, the local concentration over the surface of the sphere stays almost constant with time and for a diffusion limited case, $Da \gg 1$, the diffusive flux of reactants is not able to compensate for the fast reaction and the concentration decreases quickly near the catalytic surface, see Fig. 6. For fast-reactions, the dimensionless half-life of the reactant concentration near the catalytic surface occurs approximately over the time scale $t^o = 1/(1+Da)^2 \approx 1/Da^2$ where $t^o = 1$ represents time scale for diffusion over a length scale of sphere radius. The logarithm of the dimensionless half-life time is plotted against the logarithm of Damkohler number, Fig. 7.

Fig. 8 shows the concentration of A as a function of distance r^o away from the sphere after a diffusive time scale, $t^o = 1$ for different Damkohler numbers.

It becomes a computational challenge to tackle a simple reaction-diffusion case when $Da \ll 1$ or $Da \gg 1$. As has been observed in this example, SRD is quite efficient in resolving the two processes even when they occur at complete different time scales. Next step is to introduce a third time scale into our problem, the convective time scale.

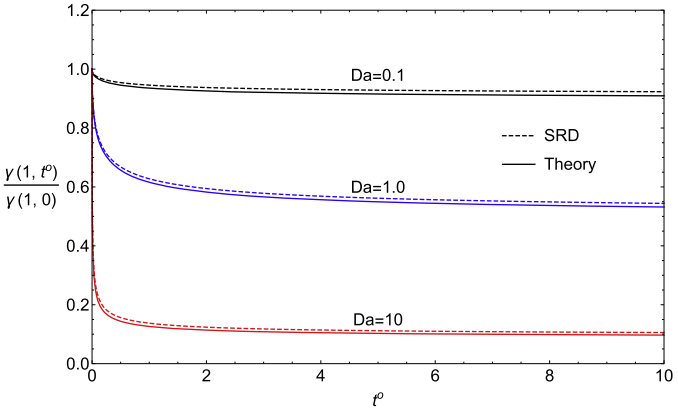

Fig. 6. Change in local concentration of reactant A at $r^o = 1$ with time t^o for 3 Damkohler numbers, $Da = 0.1, 1.0, 10$. $Da = k^{A,o}_{ads}$ for a linear assumption of reaction. Theory Eq. (13) versus SRD predictions.

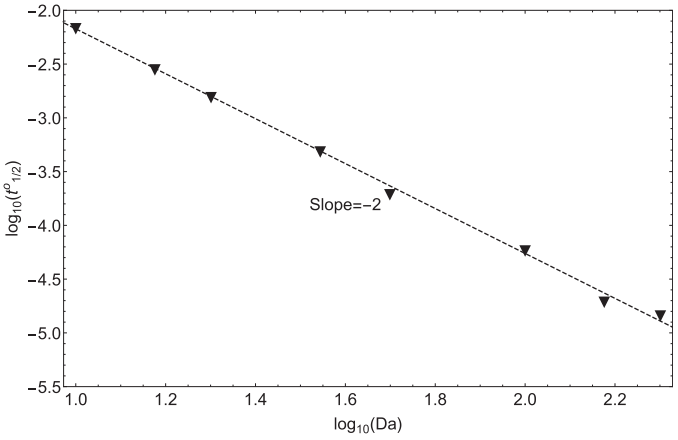

Fig. 7. Logarithm of half-life time of reactant concentration as a function of logarithm of the Damkohler number.

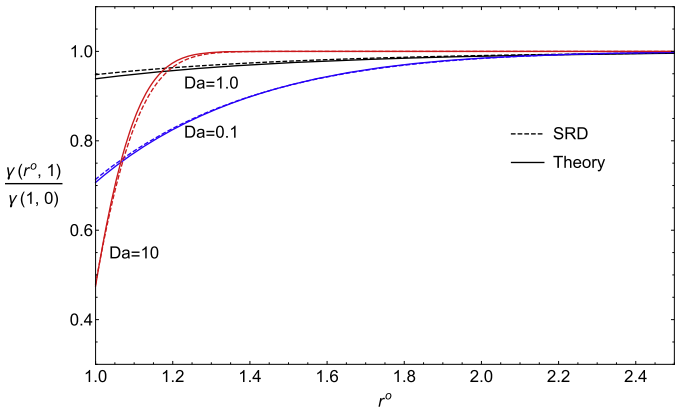

Fig. 8. Change in concentration of reactant A with distance r^o at $t^o = 1$. Theory Eq. (13) versus SRD predictions.

3.5. Dispersion with reaction in a packed bed

Up to this point, we have validated the model for at most two competing processes (reaction - diffusion, convection - diffusion) at the same time. Now, we introduce a linear reaction, as described in Section 3.4, over the surfaces of all spheres in the packed bed, as defined in Section 3.3, and study conversion across the reactor length as a function of the interplay between convection, diffusion and reaction.

The system, see Fig. 5, has periodic boundaries at $x = 0, x = L_x, y = 0, y = L_y, z = 0, z = L_z$. The direction of flow is the z-direction. To neglect transverse dispersion effects, we will always ensure that $L_z/L_x > 10$, $L_z/L_y > 10$ (Klinkenberg et al., 1953; Delgado, 2006). For gas-like fluids, the longitudinal dispersion D_L depends on the bulk diffusivity of the fluid components, the average fluid velocity and the sphere diameter (Gunn, 1987; Alves et al., 2006; Delgado, 2006):

$$\frac{D_L}{D_A} = \frac{1}{\tau'} + \frac{1}{12}\frac{u(2R)}{D_A} \tag{15}$$

where τ' is the tortuosity of the packed bed column and u is the average fluid velocity in the longitudinal direction. For a packed bed of spheres, we can set $\tau = \sqrt{2}$ (Lanfrey et al., 2010). Non-dimensionalizing Eq. (15) with the help of Table 3, we find

$$D^o_L = \frac{1}{\tau'} + \frac{u^o}{6} \tag{16}$$

We will consider a three-component system, containing a majority inert solvent species S, a reactive species A which can adsorb over the surface of the catalytic spheres and undergo a reaction, to produce product species B. For a linear reaction, the reaction rate constant will be k^A_{ads}. A, B and S only differ by a tag therefore we can make the simplifying assumption of constant diffusivity/dispersion across the axial direction as long as Re is not too high (< 200).

The reactor is full of solvent particles S at the start of system $t = 0$. We maintain a constant pressure difference for all $t > 0$ and let the system attain mechanical equilibrium, similar to Section 3.3. This initial run time of the setup is time t_{start}.

For all $t > t_{start}$, the following two processes occur. Firstly, as solvent S starts to move out of the system at $z = L_z$, it is made to

re-enter from the boundary at $z = 0$ as species A. For more information about mass and momentum conservation when carrying out this step for different mass particles, see Appendix C. As species A starts to fill the reactor, the reaction over the sphere starts with rate k^A_{ads} producing species B. As has been discussed in the previous section, for a linear assumption of reaction, B once formed will not desorb back on any catalytic sphere and eventually exit the system from $z = L_z$. For every particle B leaving the system, a particle A re-enters the system from $z = 0$. As the reaction progresses, the system will develop a distribution of S, A, B along the reactor length. Any species that diffuses back and leaves the system at $z = 0$ will be reintroduced from the boundary at $z = L_z$ as the same species. However, such an implementation will also result in B formed at the start of the reactor to re-enter the reactor from $z = L_z$ after diffusing backwards, affecting the output concentration of reactants or products.

To remove this effect, we define inert inlet and outlet regions of length L near the boundaries in the z-direction whose dimension should be at least the minimum of L_y, L_x (Deprez and de Buyl, 2017). Species A will only react between $z = L$ and $z = L_z - L$. This inlet region gives the product species B, formed just near the inlet region, some space to diffuse back (without leaving the system) and eventually be convected away by the flow in $+z$ direction.

The simplifications involved in resolving the system into three primary time scales are the following. Firstly, the catalyst should equilibrate almost instantaneously, as compared to convective and reactive time scales, to avoid depletion region formation near the catalyst and also to ensure the reaction remains linear (Sengar et al., 2017). Secondly, the time taken for particles to disperse across one box-length in the transverse direction (x, y) should be comparable or more than the time taken for particles to convect across the reactor length in the flow direction.

The variation of the number density of reactant species A along the z direction can now be written as

$$D_L \frac{d^2\gamma_A}{dz^2} - u\frac{d\gamma_A}{dz} + r_A = 0 \tag{17}$$

where u is the steady state velocity of solvent particles S at $t = t_{start}$ (under our assumptions, the system distribution of velocities of particles across the reactor for $t < t_{start}$ and $t > t_{start}$ will be the same) and r_A is the rate of consumption of A per unit volume per unit time, $r_A = -k\gamma_A$. Note that the previously mentioned k^A_{ads} differs from the current k. We can derive its value as follows.

Consider a cross-sectional volume element of length Δz along z direction and L_x, L_y along x and y direction respectively. For sufficiently high number of spheres in the model reactor, the total number of catalytic spheres in this volume element will be equal to $N_{\Delta z} = N_s \Delta z / L_z$. If the adsorption flux of A on a single sphere inside this volume element is $k^A_{ads}\gamma_A(t)A_{cat}$, the adsorption flux of A in the volume element will be $k^A_{ads}\gamma_A(t)A_{cat}N_s\Delta z/L_z$. The volumetric adsorption flux $k\gamma_A(t)$ will be

$$k\,\gamma_A(t) = \frac{k^A_{ads}A_{cat}N_s}{L_xL_yL_z}\gamma_A(t) \tag{18}$$

$L_xL_yL_z$ is the volume of the model reactor, $A_{cat} = 4\pi R^2$ and N_s, the total number of catalytic spheres, can be related to the total reactor volume as

$$\frac{4}{3}N_s\pi R^3 = (1-\epsilon)L_xL_yL_z \tag{19}$$

Using Eqs. (18) and (19), we can write the volumetric reaction rate constant as

$$k = \frac{3}{4}\frac{k^A_{ads}(1-\epsilon)}{R} \tag{20}$$

and the dimensionless volumetric reaction rate constant is

$$k^o = \frac{3}{4}k^{A,o}_{ads}(1-\epsilon) \tag{21}$$

An analytical solution for Eq. (17) has been presented in Levenspiel (1962). The reactant concentration $\Psi(z) = \gamma_A(z)/\gamma_{A,0}$ across the length of the reactor $\lambda = z/L_z$ is

$$\Psi = \frac{(1+q)\exp\left(\frac{q}{2}Pe_L(1-\lambda)\right) - (1-q)\exp\left(-\frac{q}{2}Pe_L(1-\lambda)\right)}{(1+q)^2\exp(\frac{q}{2}Pe_L) - (1-q)^2\exp(-\frac{q}{2}Pe_L)} \tag{22}$$

where $q = \sqrt{1 + 4Da_L/Pe_L}$. $Pe_L = u^oL^o_z/D^o_L$ is the dimensionless Peclet number relating the convection and dispersion time scales along the longitudinal length in the reactor. $Da_L = k^oL^o_z/u^o$ is the Damkohler number relating the reaction and convection time scales along the longitudinal direction over a length L. Note the difference with the Damkohler number defined in Section 3.4 which related the reaction and diffusion time scales over a single sphere radius.

Fig. 9 plots the variation of reactant concentration along the reactor length for $Da_L = 1.0$ and $Da_L = 10.0$, respectively. For the present simulation framework, the reaction occurs between $z = L$

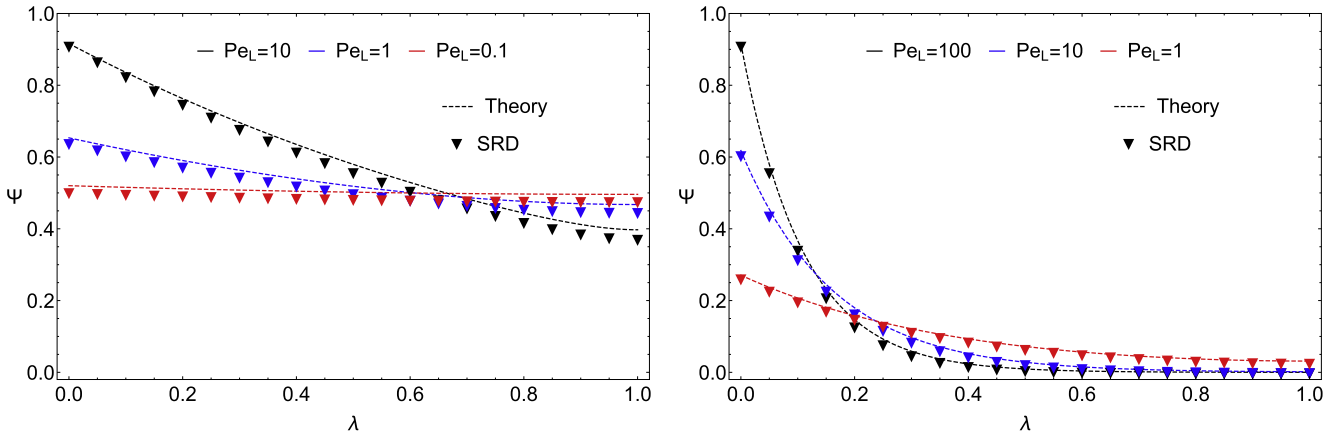

(a) $Da_L = 1.0$ (b) $Da_L = 10$

Fig. 9. Variation of reactant concentration, $\Psi(z) = \gamma_A(z)/\gamma_{A,0}$, along the length of the reactor, $\lambda = z/L_z$. Dashed line is the analytical solution from Eq. (22), and inverted triangles are the solution points from SRD simulations. Note that the Da_L and Pe_L values obtained are approximately close to their actual values since the input parameters have to be tuned to generate output variables(Da_L, Pe_L) that are related to each other by a common variable u^o.

Table 4
Variable parameter set used to predict the different dimensionless number sets. All units have been non-dimensionalized according to Table 2

Dimensionless numbers	Parameter set
$Da_L = 1, Pe_L = 0.1, Re = 0.087$	$g^o = 0.05, p^A_{ads} = 0.002, L'^o_z = 10$
$Da_L = 1, Pe_L = 1, Re = 0.43$	$g^o = 0.27, p^A_{ads} = 0.004, L'^o_z = 20$
$Da_L = 1, Pe_L = 10, Re = 3.2$	$g^o = 2.0, p^A_{ads} = 0.02, L'^o_z = 30$
$Da_L = 10, Pe_L = 1, Re = 0.87$	$g^o = 0.55, p^A_{ads} = 0.15, L'^o_z = 10$
$Da_L = 10, Pe_L = 10, Re = 4.9$	$g^o = 3.1, p^A_{ads} = 0.45, L'^o_z = 20$
$Da_L = 10, Pe_L = 100, Re = 21$	$g^o = 13.8, p^A_{ads} = 0.5, L'^o_z = 75$

and $z = L_z - L$, so the effective reactor length should be $L'_z = L_z - 2L$. However, figures are provided by mapping the modified reactor length, L'_z over the real reactor length L_z make it convenient to analyze.

All the simulations in Fig. 9 have the following fixed dimensionless parameters (refer to Section 3.1 and Table 2): $\gamma^o_A = 3000, \Delta t^o_c = 0.07, m^o_A = 0.00045, N_s = 1000, L^o_x = L^o_y = 10, L^o_z = 100$, $\epsilon = 0.5$. The base units are $R = 4.47a_0$, $\eta_A = 15.27m_0/(t_0a_0), D_A = 2.07a_0^2/t_0$.

For an SRD fluid, the corresponding Schmidt number, Sc under the given $\gamma^o_A, \Delta t^o_c, m^o_A$ is 0.2 representing a gas-like fluid behavior ($H_{2,g}$). All simulations predict Reynolds number $Re < 100$. Table 4 highlights the variables parameters used to obtain the different Da_L and Pe_L.

For $Da_L < 1$, the reaction time scales are longer than the convective time scales, which makes the situation uninteresting to present here (but is generally observed in many real chemical reactors). When $Da_L \geqslant 1$, the boundary layer length around the catalytic spheres will determine the concentration of A. When $Pe_L > Da_L$, diffusion is the slowest process. Convection resists reaction at the start of the reactor but due to the small boundary layers of reactant around the spheres, reaction is supported along the length of the reactor. When $Pe_L \ll 1$, convection becomes slower than diffusion and the reactor behaves like a CSTR.

4. Nonlinear reactor models

In Section 3, we have validated the SRD model for first order reaction system when the mass diffusivity of the reactants equals the mass diffusivity of the products. In this section, we consider a model reactor as described in Section 3.5 and present two situations where (a) reaction order is nonlinear, and (b) product diffusivity is different from reactant diffusivity.

4.1. Binary nonlinear reaction system

In our previous study (Sengar et al., 2017), we have described the need for Langmuir-Hinshelwood type of kinetics to model a simple reaction system like $A \rightarrow B$.

$$A \underset{k^A_{des}}{\overset{k^A_{ads}}{\rightleftharpoons}} A* \xrightarrow{k^A_r} B* \underset{k_{onB}}{\overset{k^B_{des}}{\rightleftharpoons}} B$$

The rate equations for this model are:

$$N_{cat}\frac{d\theta_A}{dt} = k^A_{ads}\gamma_{A,l}\theta - k^A_{des}N_{cat}\theta_A - k^A_r N_{cat}\theta_A \tag{23a}$$

$$N_{cat}\frac{d\theta_B}{dt} = k^A_r N_{cat}\theta_A - k^B_{des}N_{cat}\theta_B + k^B_{ads}\gamma_{B,l}\theta \tag{23b}$$

Under a pseudo-steady state assumption, a catalytic surface is locally assumed to be equilibrated. The steady-state fractional occupations of A and B, respectively, are:

$$\theta_{A,eq} = \frac{K^A_{eq}\gamma_{A,l}}{1 + K^A_{eq}\gamma_{A,l} + K^B_{eq}\gamma_{B,l} + k^A_r\left(\frac{K^A_{eq}\gamma_{A,l}}{k^B_{des}} + \frac{K^B_{eq}\gamma_{B,l}}{k^A_{des}} + \frac{1}{k^A_{des}}\right)} \tag{24}$$

$$\theta_{B,eq} = \frac{K^B_{eq}\gamma_{B,l} + k^A_r\left(\frac{K^A_{eq}\gamma_{A,l}}{k^B_{des}} + \frac{K^B_{eq}\gamma_{B,l}}{k^B_{des}}\right)}{1 + K^A_{eq}\gamma_{A,l} + K^B_{eq}\gamma_{B,l} + k^A_r\left(\frac{K^A_{eq}\gamma_{A,l}}{k^B_{des}} + \frac{K^B_{eq}\gamma_{B,l}}{k^A_{des}} + \frac{1}{k^A_{des}}\right)} \tag{25}$$

where $K^i_{eq} = k^i_{ads}/N_{cat}k^i_{des}$ and $\gamma_{i,l}$ represents the number density of species i locally over the catalytic strip.

The rate of disappearance of A at this pseudo-steady state is $k^A_{ads}\gamma_{A,l}\theta_{eq} - k^A_{des}N_{cat}\theta_{A,eq}$ which is equal to the rate of generation of B, $-k^B_{des}N_{cat}\theta_B + k^B_{ads}\gamma_{B,l}\theta_{eq}$ which in turn is equal to the rate of surface reaction $k^A_r N_{cat}\theta_{A,eq}$.

In Section 3.5, the kinetics equations were written under the condition $p^A_{des} = 0.0, p^A_r = 1.0, p^B_{des} = 1.0, p^B_{ads} = 0.0$. The rate of disappearance of A then becomes $k^A_{ads}\gamma_{A,l}$ (for any p^A_{ads}). This linearity assumption generates a Damkohler number which is a constant across the reactor system. This might not be the case when the probability parameters mentioned above change. We will now use the probability parameters defined to generate Fig. 9 as the base case and compare the scenarios when p^B_{ads} and p^B_{des} changes.

The setup of the reactor is the same as described in Section 3.5. Previously, the equilibration time of the catalyst was zero. This enabled us to assume a steady state concentration of reactants and products across the reactor already after a time $t_{start} + t_{reactor}$ where $t_{reactor} = L_z/u$, the typical residence time of particles inside the reactor.

Now, we also have to account for the equilibration lifetime, t_{eq}, of each catalytic surface present in our system. We can, approximately, determine this lifetime as follows. When $k^A_r \rightarrow 0$, the equilibration lifetime is of the order of $\text{Max}\{(k^A_{ads}\gamma_{A,l}/N_{cat} + k^A_{des})^{-1}, (k^B_{ads}\gamma_{B,l}/N_{cat} + k^B_{des})^{-1}\}$. Similarly, when $k^A_r \rightarrow \infty$, the equilibration lifetime is of the order $\text{Min}\{(k^A_{ads}\gamma_{A,l}/N_{cat} + k^A_{des})^{-1}, (k^B_{ads}\gamma_{B,l}/N_{cat} + k^B_{des})^{-1}\}$. Using this analysis, we can always predetermine a suitable time after which every catalyst can be assumed to be equilibrated.

Now, at time $t = t_{start} + t_{reactor} + t_{eq}$, we analyse the steady state concentration profiles of the reactants and the products.

Fig. 10 shows the deviation from the linear assumption for 2 cases, Da_L = 1.0, Pe_L = 10.0 and Da_L = 10.0, Pe_L = 10.0 (shown by thick black lines in both figures) as probability parameters change.

In Fig. 10(a), p^B_{des} is fixed at 0.01 and p^B_{ads} is varied from 0 to 0.9. p^A_{ads} is kept constant (see Table 4). For p^B_{ads} = 0.0, the adsorption of reactant A is still the slowest process and the curve almost overlaps with the base case. As p^B_{ads} increases, the readsorption flux of product B increases along the length of the reactor. This, in turn, shifts the fractional coverage over the catalyst in favor of B. The effect is visible in the concentration of A along the reactor length since more unreacted A is now convected along the longitudinal direction.

For Fig. 10(b), p^B_{ads} is fixed at 0.5 and p^B_{des} is varied from 0 to 0.9. The higher desorption probability of B allows more reactant species A to adsorb, and consecutively react to form product B.

4.2. Unequal species diffusivity

In the previous section, a nonlinear reaction was analyzed while ensuring that the diffusivity of the mixture in the bulk of the

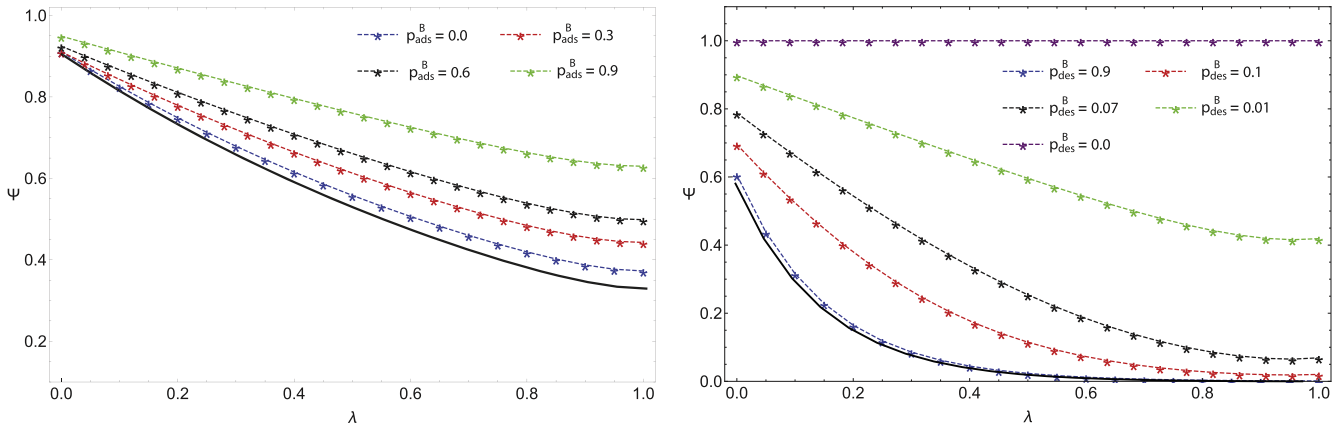

(a) $Da_L = 1.0, Pe_L = 10.0$ (b) $Da_L = 10, Pe_L = 10.0$

Fig. 10. Variation of reactant concentration, $\Psi(z) = \gamma_A(z)/\gamma_{A,0}$, along the length of the reactor, $\lambda = z/L'_z$. Dashed line is the fit obtained for the starred points where concentration in model reactor is calculated. The thick black line in both cases represent the base case for $Da_L = 1.0, Pe_L = 10.0$ and $Da_L = 10.0, Pe_L = 10.0$ respectively. (a) Effect of altering probability of readsorption of B with $N_{cat} = 100, p^B_{des} = 0.01$, (b) Effect of altering probability of surface reaction of A to B with $N_{cat} = 100, p^B_{ads} = 0.5$. The rest of simulation parameters are same as used in Fig. 9.

reactor system always remains the same. Now, we will study the system when the reactant and product species have different diffusivity values.

With the same reactor model as defined in Section 3.5, we initiate a reaction $A \rightarrow nB$. Consequently, $m_A = m_B/n$ where $n > 1$ or $n < 1$. For an SRD fluid, changing the mass of particles inversely affects their diffusivity, Eq. (1). Since we are mainly interested to measure the effects of bulk diffusivity in the mixture, a first-order reaction is considered ($p^A_{ads} > 0, p^A_{des} = 0.0, p^A_r = 1.0, p^B_{des} = 1.0, p^B_{ads} = 0.0$).

We consider the case Da_L = 1.0, Pe_L = 10.0 with the same simulation parameters as used to generate the corresponding curve in Fig. 9. The rules for conversion of A to B on the catalytic surface, when mass of the two species is different, is mentioned in Appendix C. Appendix C also mentions the conservation rules applied to handle boundary conditions when particles A or B leave the periodic boundaries (as defined in Section 3.5).

When $m_B < m_A$, the mutual diffusivity of the mixture is higher than the self-diffusivity of reactant A. This translates to a lower frictional force experienced by A while traversing the reactor, thereby, reducing the residence time of species A between a volume element z and $z + dz$. This effect is visible in Fig. 11 where for $m_B < m_A$, more unreacted A is present along the reactor length as compared to the situation with $m_B = m_A$. For $m_B > m_A$, the effect is reversed and the mobility of A decreases.

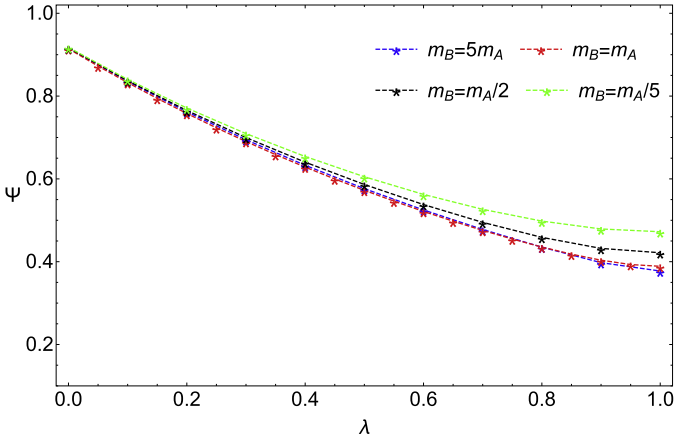

Fig. 11. Variation of reactant concentration, $\Psi(z) = \gamma_A(z)/\gamma_{A,0}$, along the length of the reactor, $\lambda = z/L'_z$. Dashed line is the fit obtained for the starred points where concentration in model reactor is calculated. Simulations are performed when $m_B \neq m_A$ and compared with the base case with $m_B = m_A = 1.0$ (red dashed line) for $Da_L = 1.0, Pe_L = 10.0$ of Fig. 9. (For interpretation of the references to colour in this figure legend, the reader is referred to the web version of this article.)

It should also be noted that the above reaction system does not conserve the number of particles in the system which is a source of an internal pressure difference generated along the longitudinal direction. This pressure adds up to the external pressure difference when $m_B < m_A (n > 1)$. Conversely, when $m_B > m_A (n < 1)$, this internal pressure goes against the external pressure. This effect itself can be incorporated into the Maxwell-Stefan diffusivity between A and B. Further information is provided in Appendix D.

5. Discussion and conclusion

We have presented here a multiscale modeling technique that is able to accurately resolve different processes occurring on time scales that differ on orders of magnitude. We have highlighted the basic modeling techniques involved in modeling a simple reactor system (involving convection, diffusion and reaction) using SRD. The analysis was first carried out for a linear reaction assumption, followed by the incorporation of a reaction cycle following Langmuir Hinshelwood kinetics. The ability of the SRD model to also account for multicomponent diffusion opens up a whole new domain of complex reaction system that can be modeled.

To model a real chemical reactor, the number of processes occurring at different time scales might be much larger than 3. Even if kinetics is given by the simple Langmuir Hinshelwood model, intermediary processes like adsorption, desorption, surface reaction become important. As the number of participating components increase, the system complexity increases and resolution of each and every process becomes challenging.

The generation of different product species in such a multicomponent nonlinear scheme will directly affect the behavior of the bulk fluid as well. Different species in the bulk will have different self-diffusivity. The pairwise interaction between species can be incorporated in a mutual diffusivity expression, which has been presented in this work, using SRD, for a binary mixture but can be extended for any n component solution. Unequal moles of reactants and products might lead to an internal pressure force originating from or away from the reaction site, the contribution of which has been incorporated in the Maxwell-Stefan diffusion coefficients, see Appendix D.

Another time scale of importance is the equilibration time of the catalytic strip. For all cases with linear reaction assumption, we assumed that the catalyst equilibrates or achieves a pseudo steady state instantly. When this is not observed, regions of low density (depletion regions) may form near the catalytic strip which can be a source of another driving force(only for higher values of *Sc*). When reactions occur inside complex geometries, a new time scale will be present which relates to the time taken for the reactant fluid to move through a pore towards the reaction site (pore diffusion).

The combined effect of the above described processes is reflected in the output concentration of any species from the reactor system. A macroscale reactor might involve length scales much larger than the length scales of individual processes which will result in the incorporation of another time scale in the system.

With a large number of processes to resolve at the hydrodynamic and reaction level, SRD has been shown to be quite effective in resolving particle-particle interactions quickly for a large number of components. The computational efficiency of the algorithm therefore makes it easy to couple this scheme with any reaction-based scheme for complex geometries, as long as the reaction steps conform to the mean-field assumption.

We would like to end the discussion for this work by guiding the readers interested in further resolving the system of interest. For reaction schemes where a mean-field assumption does not hold true (island formation or phase transition at the catalytic sites), a stochastic treatment to the individual reaction steps has to be done which will add up to the simulation time. For such complex reaction schemes, one may use Machine Learning to develop an algorithm that observes a stochastic reaction cycle. The algorithm is then able to predict the output fractional vacancies of different species based on input of (a) reaction rate constants at time t, (b) fractional vacancy of surface sites at time t, and (c) the hydrodynamic time step Δt_c. This will be the topic of our future work.

Acknowledgement

The work is part of the Netherlands Center for Multi-scale Catalytic Energy Conversion (MCEC), funded by the Netherlands Organization for Scientific Research, NWO.

Appendix A. Reactions on a sphere

To model reactions over a more complex geometry like a sphere, the lattice cells in an SRD fluid near boundaries should be updated and the catalytic surface needs to be modified.

To simulate a catalytic sphere with periodic boundaries, the surface of the sphere will be no-slip and reactive. As mentioned before, a grid-shift procedure helps achieve Galilean-invariance in the system where lattices are shifted in space before collision by a random number between 0 and a_0 in each Cartesian direction. Due to this, all lattice cells inside the sphere which are at a distance $\sqrt{3}a_0$ from the surface need to be checked for ghost-cell boundary conditions. For all cells near boundaries, a modified ghost boundary cell approach was used that conserves not the number density of particles but the average centre of mass momentum of particles in the bulk (Sengar et al., 2017).

In presence of convection, the pressure over the sphere will be different at different positions. A single averaged catalytic surface will then give wrong predictions. To tackle this, the surface of the sphere can be divided into α surfaces. Assuming a flow in z direction, there is azimuthal symmetry in the system along the z axis. Hence, the sphere surface can best be divided into α strips with equal areas such that $\alpha A = 4\pi R^2$ where A is the area of a single divided strip and R is the radius of the sphere. It is known that dividing a sphere into α equal parts along any Cartesian axis will result in an equal surface area of each portion.

Appendix B. Coupling reactions with hydrodynamics

In our previous work, Sengar et al. (2017), we outlined the need to rewrite the rate equations to simultaneously simulate adsorption, desorption and reaction steps. Let's assume adsorption of A on a catalytic strip, the rate equations when coupled with the fluid in the bulk can be written as

$$\frac{\Delta\theta_A}{\Delta t_c} = k_1\theta - k_2\theta_A - k_3\theta_A + k_4\theta_B \tag{B.1a}$$

$$\frac{\Delta\theta_B}{\Delta t_c} = k_6\theta + k_3\theta_A - k_4\theta_B - k_5\theta_B \tag{B.1b}$$

where Δt_c is the hydrodynamic time step of the fluid and $\theta = 1 - \theta_A - \theta_B$ by the conservation of surface sites. The hydrodynamic time step is set such that the adsorption rates k_1 and k_6 (of A and B respectively) can be assumed constant over this time period. If this is not the case, Δt_c needs to be reduced further. Sequential treatment of the reaction steps might lead to overestimation or underestimation of a surface species concentration. This occurs if the change produced by any intermediary step in the reaction cycle within one time step is much higher as compared to the other steps (which generally occurs when reaction occurs much faster than diffusion). For an accurate simultaneous representation of the reaction system, one solution is to reduce the time step Δt_c. This however increase the computational time. In this work, we use a technique that modifies the instantaneous rates at every time step to avoid any error.

B.1. Adaptive rate method

We define the fastest intermediary step between time interval t and $t + \Delta t_c$ as $\psi(t) = Max(k_i\theta_j)$. The method involves rewriting the rate equations with respect to the process k_i acting on θ_j. The modified rate equations then become

$$\frac{\Delta\theta_A}{\Delta t_c} = \psi(t)\left(k'_1\theta - k'_2\theta_A - k'_3\theta_A + k'_4\theta_B\right) \tag{B.2a}$$

$$\frac{\Delta\theta_B}{\Delta t_c} = \psi(t)\left(k'_6\theta + k'_3\theta_A - k'_4\theta_B - k'_5\theta_B\right) \tag{B.2b}$$

where $k'_i = k_i/\psi(t)$. For every time step t, the rate constants of the all intermediary steps are modified by $\psi(t)$. The reaction cycle is initiated by the first occurrence of $\psi(t)$ following which a sequential treatment of the other processes with modified rate occurs. This is repeated until all the occurrences of $\psi(t)$ are exhausted.

As discussed in Sengar et al. (2017), the adsorption probabilities derived from the adsorption rates remain independent of the steaming step of the fluid, $p^i_{ads} = ck^i_{ads}$ where c is a constant that depends on simulation parameters and fluid properties (Table 3). The modified adsorption probability for the scheme discussed becomes $p'_{ads} = ck'_{ads}C_s$. The probability of desorption and reaction/-conversion to other surface species is linked to the rate constants as $p_{des} = -\log(1 - k_{des}\Delta t_c)$. The modified probability then becomes $p'_{des} = -\log(1 - k'_{des}\Delta t_c)$.

A reaction cycle involving nonlinear reaction pathways, for example $k\theta_A\theta_B$, can be easily modified using the above approach. The modified rate can be written as $k' = k\theta_A/\psi(t)$, and a probability parameter can be obtained for the modified rate constant. Since $k' \leqslant k$, the linearization approach used to model with scheme Eq. (B.2) will always be numerically more accurate that sequential treatment in Eq. (B.1).

B.2. Matrix formulation

The second method involves writing the rate of change in surface species involved in matrix formulation and solving it numerically over the streaming time step of the fluid.

$$\begin{bmatrix} \Delta\theta/\Delta t_c \\ \Delta\theta_A/\Delta t_c \\ \Delta\theta_B/\Delta t_c \end{bmatrix} = \begin{bmatrix} -k_1-k_6 & k_2 & k_5 \\ k_1 & -k_2-k_3 & k_4 \\ k_6 & k_3 & -k_4-k_5 \end{bmatrix} . \begin{bmatrix} \theta \\ \theta_A \\ \theta_B \end{bmatrix}$$

The above matrix calculates the surface species concentration at the end of time step Δt_c. With this information, we can numerically predict the total number of adsorptions, desorptions and reactions to occur over the catalytic strip between time t and $t+\Delta t_c$. If $\Delta\theta_{i,j}$ represents the number of occurrences of reaction step k_i acting over θ_j between time t and $t+\Delta t_c$, the modified probability for any process becomes $\Delta\theta_{i,j}/\theta_j(t)$. If $\Delta\theta_{1,A}$ is the numerically calculated number of adsorptions of species A between t and $t+\Delta t_c$, the modified probability of adsorption for time t is $\Delta\theta_{1,A}/\theta_A(t)$.

For a nonlinear rates like $k\theta_A\theta_B$ with number of occurrences between t and $t+\Delta t_c$ equal to $\Delta\theta_{A,B}$, the modified probability will be $\Delta\theta_{A,B}/\theta_A(t)$ or(and) $\Delta\theta_{A,B}/\theta_B(t)$ depending on which surface species is (are) affected.

Appendix C. Mass and momentum conservation

The modeled system involving a reaction has two primary regions where SRD particles change to a different species while conserving mass and/or momentum. At the catalytic sites where the reaction occurs, a change in number of product particles with mass conservation occurs. Secondly, at open boundaries if particles change nature(from products to reactants or vice versa), mass and momentum conservation rules need to be applied.

C.1. Adding particles

We explore the mass and momentum conservation rules for the case where addition of $n>1$ particles of different mass and velocity leads to the formation of a single new particle.

By mass conservation,

$$m' = \sum_{i=1}^{n} m_i \tag{C.1}$$

where m_i is the mass of initial particles and m' is the mass of the new particle.

Let the velocity of individual particles be $v_i + dv_i$ where v_i and dv_i are the first and second moment of velocity respectively.

To generate $v' + dv'$ as the velocity of new particle, we perform momentum conservation, $m'v' = \sum_{i=1}^{n} m_i v_i$ which gives the first moment of velocity of the new particle as

$$v' = \frac{\sum_{i=1}^{n} m_i v_i}{\sum_{i=1}^{n} m_i} \tag{C.2}$$

Since the temperature of the ensemble of SRD particles is stored in the velocity fluctuations of each particle, we need to generate the second moment of velocity of new particle such that the total energy of the system is preserved. The total energy of all initial particles is:

$$E_{initial} = \sum_{i=1}^{n} m_i dv_i^2 \tag{C.3a}$$

$$E_{initial} = \sum_{i=1}^{n} m_i \frac{k_B T}{m_i} = n k_B T \tag{C.3b}$$

By conservation of energy, $E_{initial} = E_{final}$.

$$E_{final} = m' dv'^2 \tag{C.4a}$$

$$m' dv'^2 = n k_B T \tag{C.4b}$$

$$dv' = \sqrt{\frac{k_B T}{m'/n}} \tag{C.4c}$$

The above equation implies that the new particle formed should be given a random velocity fluctuation from a normal distribution with standard deviation $\sqrt{\frac{k_B T}{m'/n}}$ to conserve total energy of the system. Note that m'/n is just the average masses of the initial particles.

C.2. Splitting particles

Splitting a single particle, with mass m', velocity v' and velocity fluctuation dv', requires the same approach as above: conservation of mass, momentum and velocity fluctuations (leading to energy conservation). If $n>1$ new particles are created with mass m_i, by mass conservation,

$$m' = \sum_{i=1}^{n} m_i \tag{C.5}$$

If the velocity of ith particle is $v_i + dv_i$, where v_i is the mean velocity and dv_i is the velocity fluctuation, by momentum conservation,

$$m'v' = \sum_{i=1}^{n} m_i v_i \tag{C.6}$$

The energy of the initial particle $E_{initial}$ is $k_B T$. The energy of final particles E_{final} (which is equal to $E_{initial}$ is

$$E_{final} \sum_{i=1}^{n} m_i dv_i^2 = k_B T \tag{C.7}$$

A solution to the above equation is $dv_i^2 = k_B T/m'$. Therefore, we can generate a velocity fluctuation for all the new particles from a normal distribution of standard deviation $\sqrt{k_B T m'}$. The implication of this is that new particles formed are at a lower temperature than the initial particle by a fraction $\sqrt{m_i/m}$. Within a few collisional steps, these new particles will equilibrate according to their Maxwellian distribution with a second moment of velocity $k_B T/m_i$ (if the environment around this particle consists majorly of particles of mass m_i).

C.3. Updating particle positions

In case of adding particles, only particles in the vicinity of half a cubic cell length $a_0/2$ are combined together since a velocity gradient present along any direction might lead to particles adding from regions of very different velocities. Following this, the coordinates of the new particle should be the coordinates of the center of mass of all the other particles.

$$m'\mathbf{r}' = \sum_{i=1}^{n} m_i \mathbf{r_i} \tag{C.8}$$

When splitting particles, since the velocity of new particles is the same as the initial particle, new particles can be positioned at the same location as the initial particle. This creates a region with high number density and low individual temperature of the formed particles momentarily until they distribute their mass in the bulk and attain the same temperature as the bulk.

Appendix D. Maxwell-Stefan diffusion: unequal consumption and generation over catalyst

Chemical reactions might involve change in pressure at the reaction site as compared to the bulk if total moles of gaseous product species is different than total moles of reactant product species. A pressure difference towards or away from the catalyst will affect the diffusivity of whole region. To demonstrate this aspect, we use the simulation method used in Sengar et al. (2017).

To summarize, a reaction $A \rightarrow nB$ occurs at a catalytic strip, placed along the z axis of a 3D box ($L_x \times L_y \times L_z$) with walls along y direction and open boundaries along the x and z direction. The reaction leads to change in number of particles and mass of particles, leading to change in diffusivity of product particles, Eq. (1). The catalytic strip with dimensions $L_x \times L_{cat}$ is placed at the center of the box along the $y = 0$ wall such that length of strip in z direction is small as compared to the length of the box, L_z. At $z = 0$ and $z = L_z$ product particles B are removed following the conservation principles defined in Appendix C. At $x = 0$ and $x = L_x$, particles are re-entered into the system from the other end without any change in their physical property. There is no convection, only diffusion leading to transient velocity gradients that disappear at steady state. The net force on a particle of reactant or product species i can be written as Taylor and Krishna (1993)

$$RT\mathbf{d_i} = \nabla_T \mu_i - \mathbf{F}_i \tag{D.1}$$

where $\nabla_T \mu_i$ is the gradient in chemical potential at constant temperature and $\mathbf{F}_i$ is the external force on the system. For the present case, the external force is a transient force that originates because of change in number of moles during a reaction. This leads to a pressure gradient in the system. At steady state the, external force becomes zero but the reaction is now supported by the pressure gradient in the system. It has been shown that under forces leading to pressure gradients in the system, the force equation can be rewritten as Taylor and Krishna (1993)

$$\mathbf{d_i} = \nabla \chi_i + (\chi_i - \omega_i)\frac{\nabla P}{P} - \frac{1}{P}\left(\gamma_i \mathbf{F}_i - \omega_i \sum_{j=1}^{n} \gamma_j \mathbf{F}_j\right) \tag{D.2}$$

where $\chi_i, \omega_i, \gamma_i$ are the number fraction, mass fraction and number density of species i and ∇P is the gradient in total pressure in the system. At steady state, the force per particle $\mathbf{d_i}$, in a system with n different species, can be equated to the diffusive flux according to the relation:

$$\gamma_t \mathbf{d} = -[B]\mathbf{J} \tag{D.3}$$

where γ_t is the total number density of particles of all species. $\mathbf{d}$ is the column matrix containing $\mathbf{d_i}$, $\mathbf{J}$ is the column matrix containing diffusive flux J_i, and B is the matrix with coefficients given by

$$B_{ii} = \frac{\chi_i}{D_{1n}} + \sum_{\substack{k=1 \\ i \neq k}}^{n} \frac{\chi_k}{D_{ik}} \tag{D.4a}$$

$$B_{ij} = -\chi_i\left(\frac{1}{D_{ij}} - \frac{1}{D_{in}}\right) \tag{D.4b}$$

where D_{ij} is the Maxwell-Stefan diffusion coefficient for species i and j or the inverse drag-coefficient experienced by species i under influence of species j. For a binary mixture, Eq. (D.3) can be written as

$$\mathbf{J_1} = -\gamma_t D_{12} \mathbf{d_1} \tag{D.5}$$

For the model reaction system involving two components, at steady state, $F_i = 0$, Eq. (D.2) can be used in Eq. (D.5) to get

$$\mathbf{J_1} = -\gamma_t D_{12}\left(\nabla \chi_1 + (\chi_1 - \omega_1)\frac{\nabla P}{P}\right) \tag{D.6}$$

The diffusive flux ($\mathbf{J}$) of reactant and product species can also be calculated at steady state of the simulation by looking at the rate of disappearance of reactant species or rate of generation of product species per square meter of the catalytic strip per unit time step which is a constant determined by the reaction rate parameters and model initialization.

When the difference in moles of product and reactant species due to reaction is small, a pressure gradient is not present and Eq. (D.6) can be written as

$$\mathbf{J_1} = -\gamma_t D_{12} \nabla \chi_1 \tag{D.7}$$

Appendix E. Computational setup

An in-house code has been developed using which all the above simulations have been performed. The present method development is a continuation of our previous work (Sengar et al., 2017) where a reaction-diffusion system was built. The present code has been developed using C and all libraries and functions have been developed within the group. The simulations run on a single core of a CPU and there is scope for both optimization and parallelization. The processor is an Intel®Xeon®E5-1650 v2 with 3.5 Ghz clock speed and 12 MB cache.

A typical simulation contains N_s spheres in a 3D box with length (L_x, L_y, L_z). Any particle undergoes the following operations: Streaming, intra-cell collision, reflection, reaction (adsorption, desorption and surface reactions).

Streaming and collision times of particles are of the same order of magnitude aad scale as $O(\gamma L_x L_y L_z)$ where γ is the typical number density of particles in the system.

To make reflections efficient, we have developed the following methodology. For each sphere in the reaction system, the lattice cells that lie inside the sphere i are tagged (0,i) and the ones that partially lie inside the spheres are tagged (1,i). This ensures an efficient calculation to predict which sphere will particles interact with based on their initial and final position (unreflected) positions (a fraction of particles that will not reflect will also get a tag (1,i)). Having done that, the higher the value of ϵ, the closer spheres will be and higher will the chance of an SRD particle to collide with the sphere will be. For increasing ϵ, we ensure that particles do not end up suffering multiple collisions between 2 spheres and we limit the number of such reflections to 3. Reflections scale up approximately as $O(\gamma L_x L_y L_z/(1-\epsilon)^2)$.

Reactions occur per single hydrodynamic time step of bulk fluid. We have defined two methodologies to perform reaction in Appendix B. In the adaptive rate methodology, we propose to perform all surface reaction operations for every instance of the fastest process. For reaction system, $O(\gamma_{avg} A_{cat} N_{cat})$ operations occur for each hydrodynamic time step where γ_{avg} is the average number density of SRD particles interacting with catalytic strip. Using the matrix formulation, the order per time step Δt_c will be $O(\gamma_{avg} A_{cat} n \Delta t_c / h)$ where h is the time-step of the runge-kutta solver used and n is the number of different surface species.

The complete runtime of a simulation is $t = t_{start} + t_{reactor} + t_{eq}$. t_{start} is the time taken to achieve mechanical equilibrium where the mean velocity across the reactor becomes fixed. Until $t = t_{start}$, only streaming, collision and reflection occur. For $t_{reactor} \approx L_z/u$, streaming, collision, reflection and reaction occur. For t_{eq}, the equilibration time of the catalyst, again all the processes occur.

For a linear process, $t_{eq} = 0$ and the simulation time generally scales because of reflections. We can also assume $t_{start} \approx t_{reactor}$. The simulation time will scale linearly on L_z/u. For $Da = 1, Pe_L = 0.1, Re = 0.087$, the simulation time was approximately 100,000 s (about a day). For $Da_L = 10, Pe_L = 100, Re = 21$, the simulation time was approximately 4000 s.

For nonlinear processes, the processes confined within L_z' dominate the system. It took approximately 100,000 s to obtain each curve of Fig. 10 (using matrix formulation). (For the same scenario in linear reactions, it took about 20,000 s per simulation) (See Table E.5).

References

Allahyarov, E., Gompper, G., 2002. Mesoscopic solvent simulations: multiparticle-collision dynamics of three-dimensional flows. Phys. Rev. E - Statis. Nonlinear Soft Matter Phys. 66 (3), 1–9.

Alves, M.A., Delgado, J.M., Guedes De Carvalho, J.R., 2006. Mass transfer from cylinders and plane surfaces buried in packed beds in alignment with the flow direction. Chem. Eng. Sci. 61 (4), 1174–1183.

Berendsen, H.J.C., 1991. Transport properties computed by linear response through weak coupling to a bath. Comput. Simul. Mater. Sci., 139–155

Chen, S., Doolen, G.D., 1998. Lattice Boltzmann method for fluid flows. Annu. Rev. Fluid Mech. 30 (1), 329–364.

Churchill, S.W., 1988. Viscous Flows: The Practical Use of Theory. Butterworths.

Collins, F.C., Kimball, G.E., 1949. Diffusion-controlled reaction rates. J. Colloid Sci. 4 (4), 425–437.

Delgado, J.M.P.Q., 2006. A critical review of dispersion in packed beds. Heat Mass Transf. 42 (4), 279–310.

Deprez, L., de Buyl, P., 2017. Passive and active colloidal chemotaxis in a microfluidic channel: mesoscopic and stochastic models. Soft Matter 13 (19), 3532–3543.

Eigenberger, G., 2008. Catalytic fixed-bed reactors. In: Handbook of Heterogeneous Catalysis. Wiley-VCH Verlag GmbH & Co., KGaA, Weinheim, Germany, pp. 2075–2106.

Gompper, G., Ihle, T., Kroll, D.M., Winkler, R.G., 2009. Multi-particle collision dynamics: a particle-based mesoscale simulation approach to the hydrodynamics of complex fluids. Adv. Polym. Sci. 221 (1), 1–87.

Gunn, D., 1987. Axial and radial dispersion in fixed beds. Chem. Eng. Sci. 42 (2), 363–373.

Huang, M.-J., Schofield, J., Kapral, R., 2016. A microscopic model for chemically-powered Janus motors. Soft Matter 12 (12), 5581–5589.

Ihle, T., Kroll, D.M., 2001. Stochastic rotation dynamics: a Galilean-invariant mesoscopic model for fluid flow. Phys. Rev. E 63 (2), 020201.

Ihle, T., Kroll, D.M., 2003. Stochastic rotation dynamics. I. Formalism, Galilean invariance, and Green-Kubo relations. Phys. Rev. E 67, 066705.

Kikuchi, N., Pooley, C.M., Ryder, J.F., Yeomans, J.M., 2003. Transport coefficients of a mesoscopic fluid dynamics model. J. Chem. Phys. 119 (12), 6388–6395.

Klinkenberg, A., Krajenbrink, H.J., Lauwerier, H.A., 1953. Diffusion in a fluid moving at uniform velocity in a tube. Ind. Eng. Chem. 45 (6), 1202–1208.

Kmiecik, S., Gront, D., Kolinski, M., Wieteska, L., Dawid, A.E., Kolinski, A., 2016. Coarse-grained protein models and their applications. Chem. Rev. 116 (14), 7898–7936.

Krishna, R., Wesselingh, J.A., 1997. Review article number 50: the Maxwell-Stefan approach to mass tranfer. Chem. Eng. Sci. 52 (6), 861–911.

Kuroki, M., Ookawara, S., Ogawa, K., 2009. A high-fidelity CFD model of methane steam reforming in a packed bed reactor. J. Chem. Eng. Jpn. 42 (Supplement), s73–s78.

Lamura, A., Gompper, G., Ihle, T., Kroll, D.M., 2001. Multi-particle collision dynamics: flow around a circular and a square cylinder. Europhys. Lett. (EPL) 56 (3), 319–325.

Lanfrey, P.Y., Kuzeljevic, Z.V., Dudukovic, M.P., 2010. Tortuosity model for fixed beds randomly packed with identical particles. Chem. Eng. Sci. 65 (5), 1891–1896.

Levenspiel, O., 1962. Chemical Reaction Engineering Third Edition. Wiley, New York.

Li, Z., Yazdani, A., Tartakovsky, A., Karniadakis, G.E., 2015. Transport dissipative particle dynamics model for mesoscopic advection-diffusion-reaction problems. J. Chem. Phys. 143 (1), 014101.

Lu, J., Das, S., Peters, E., Kuipers, J., 2018. Direct numerical simulation of fluid flow and mass transfer in dense fluid-particle systems with surface reactions. Chem. Eng. Sci. 176, 1–18.

Malevanets, A., Kapral, R., 1999. Mesoscopic model for solvent dynamics. J. Chem. Phys. 110 (17), 8605.

Noguchi, H., Gompper, G., 2008. Transport coefficients of off-lattice mesoscale-hydrodynamics simulation techniques. Phys. Rev. E - Statis. Nonlinear Soft Matter. Phys. 78 (1), 016706.

Padding, J.T., Louis, A.A., 2006. Hydrodynamic interactions and Brownian forces in colloidal suspensions: coarse-graining over time and length scales. Phys. Rev. E 74, 031402.

Pooley, C.M., Yeomans, J.M., 2005. Kinetic theory derivation of the transport coefficients of stochastic rotation dynamics. J. Phys. Chem. B 109 (14), 6505–6513.

Rohlf, K., Fraser, S., Kapral, R., 2008. Reactive multiparticle collision dynamics. Comput. Phys. Commun. 179 (1-3), 132–139.

Salciccioli, M., Stamatakis, M., Caratzoulas, S., Vlachos, D., 2011. A review of multiscale modeling of metal-catalyzed reactions: mechanism development for complexity and emergent behavior. Chem. Eng. Sci. 66 (19), 4319–4355.

Sengar, A., Kuipers, J.A.M., van Santen, R.A., Padding, J.T., 2017. Particle-based modeling of heterogeneous chemical kinetics including mass transfer. Phys. Rev. E 96, 022115.

Sheng, N., Boyce, M., Parks, D., Rutledge, G., Abes, J., Cohen, R., 2004. Multiscale micromechanical modeling of polymer/clay nanocomposites and the effective clay particle. Polymer 45 (2), 487–506.

Steinhauser, M.O., 2007. Computational Multiscale Modeling of Fluids and Solids: Theory and Applications. Springer.

Taneda, S., 1956. Studies on wake vortices (III). Experimental investigation of the wake behind a sphere at low Reynolds numbers. Rep. Res. Inst. Appl. Mech., Kyushu Univ. 4 (99105), 366.

Taylor, R., Krishna, R., 1993. Multicomponent Mass Transfer. Wiley, New York.

Tucci, K., Kapral, R., 2004. Mesoscopic model for diffusion-influenced reaction dynamics. J. Chem. Phys. 120 (17), 8262–8270.

Tüzel, E., Ihle, T., Kroll, D.M., 2006. Dynamic correlations in stochastic rotation dynamics. Phys. Rev. E 74 (5), 056702.

Tüzel, E., Pan, G., Ihle, T., Kroll, D.M., 2007. Mesoscopic model for the fluctuating hydrodynamics of binary and ternary mixtures. Europhys. Lett. (EPL) 80 (4), 40010.

Tüzel, E., Strauss, M., Ihle, T., Kroll, D.M., 2003. Transport coefficients for stochastic rotation dynamics in three dimensions. Phys. Rev. E 68 (3), 036701.

van de Ven-Lucassen, I.M.J.J., 1998. Using molecular dynamics to obtain Maxwell-Stefan diffusion coefficients in liquid systems. Mol. Phys. 94 (3), 495–503.

Vanson, J.-M., Coudert, F.-X., Rotenberg, B., Levesque, M., Tardivat, C., Klotz, M., Boutin, A., 2015. Unexpected coupling between flow and adsorption in porous media. Soft Matter 11 (30), 6125–6133.

Villemot, F., Galarneau, A., Coasne, B., 2014. Adsorption and dynamics in hierarchical metal–organic frameworks. J. Phys. Chem. C 118 (14), 7423–7433.

Wehinger, G.D., Eppinger, T., Kraume, M., 2015. Detailed numerical simulations of catalytic fixed-bed reactors: heterogeneous dry reforming of methane. Chem. Eng. Sci. 122, 197–209.